ZnO/Carbon nanowalls shell/core nanostructures as electrodes for supercapacitors

Abdelouadoud Guerra, Amine Achour, Sorin Vizireanu, Gheorghe Dinescu, Samira Messaci, Toufik Hadjersi, Rabah Boukherroub, Yannick Coffinier, Jean-Jacques Pireaux

ZnO/Carbon nanowalls shell/core nanostructures as electrodes for supercapacitors

Abdelouadoud Guerra[a,b,c,?], Amine Achour[d,??], Sorin Vizireanu[e], Gheorghe Dinescu[e], Samira Messaci[f], Toufik Hadjersi[b], Rabah Boukherroub[c], Yannick Coffinier[c], Jean-Jacques Pireaux[d]

[a] *Université Ferhat Abbas Sétif 1, El Bez, Sétif 19000, Algeria*
[b] *Centre de recherche en technologie des semi-conducteurs pour l'énergétique (CRTSE), CRTSE - 02, Bd. Dr. Frantz Fanon, B.P. 140 Alger-7, Merveilles 16038, Algeria* [c] *Univ. Lille, CNRS, Central Lille, ISEN, Univ. Valenciennes, UMR 8520, IEMN, F-59000 Lille, France*
[d] *LISE Laboratory, Research Centre in Physics of Matter and Radiation (PMR), University of Namur, BE-5000 Namur, Belgium* [e] *National Institute for Laser, Plasma and Radiation Physics, 409 Atomistilor Street, 77125 Magurele, Bucharest, Romania* [f] *Centre de Développement des Technologies Avancées (CDTA), Cité 20 août 1956 Baba Hassen, Alger, Algeria*

A B S T R A C T

In this work, carbon nanowalls (CNW) were coated with zinc oxide (ZnO) for use as supercapacitor electrodes. The ZnO layers of different thicknesses were deposited using pulsed laser ablation in oxygen reactive atmosphere. The performance of the CNW-ZnO electrodes was found to be dependent on the thickness of ZnO deposit, which in turn influences the specific capacitance and capacitance retention of the CNW-ZnO electrodes. The areal capacitance of the CNW-ZnO measured in mild electrolyte of 1 M KCl was as high as 4.3 $mF{\cdot}cm^{-2}$ at a current density of 0.2 $mA{\cdot}cm^{-2}$ and 1.41 $mF{\cdot}cm^{-2}$ at a scan rate of 10 $mV{\cdot}s^{-1}$ with an enhanced capacitance stability over 26,000 cycles. Such results demonstrate the potential use of ZnO nanostructures for low cost and high performance material for electrochemical capacitors.

1. Introduction

Electrochemical capacitors (ECs), also called supercapacitors, have attracted considerable attention due to their high power density, fast charge-discharge ability, long cycle life and environment-friendly merit compared to Li-ions batteries [1–4]. Super-capacitors are widely employed in various systems, including hybrid electric vehicles, memory back-up and renewable energy devices [5,6]. According to the known charge storage mechanism, supercapacitors can be classified into two categories: electrochemical double layer capacitors (EDLCs) and pseudo-capacitors. The charge could be stored by EDLCs (mainly restricted to carbon based materials) using charge accumulation of ions and electrons on the surface of the electrode without redox reactions [7,8]. The pseudo-capacitors, however, rely on the fast and reversible faradaic reactions of pseudo-capacitive materials, which are mainly transition metal oxides such as RuO_2 [9], VO_2 [10,11] and MnO_2 [7,8,12–15]. Indeed, transition metal oxides are considered as promising electrode materials for supercapacitors due to their higher specific capacitance compared to that of EDLCs [8,16]. Among those transition-metal oxides, zinc oxide (ZnO) has been studied with the attempt to use it as active material for ECs application thanks to its good electrochemical reactivity, eco-friendly nature [17], low cost and abundance [18,19]. However, its low specific capacitance, poor electrical conductivity as well as its moderate cyclic instability are the main obstacles for its wide application in the field of ECs [20]. These limitations could be overcome by using a template with high surface area and good electrical conductivity such as carbon nanostructures with the aim at improving the ZnO electrical conductivity and enhancing its surface area [1,2,16,17,20,21]. For example, Xiao et al. have fabricated ZnO/carbon sphere composites with an enhanced capacitive behavior, better reversible charging/discharging ability and higher capacitance values [1]. Furthermore, ZnO/graphene [2], ZnO/carbon nanofibers [16], ZnO/activated carbon [17] and ZnO/activated carbon nanofiber [20] have also been reported as ZnO@carbon composites for EC application with good capacitance and improved cycling life.

Carbon nanowalls (CNW) are emerging materials consisting of graphene nanodomains, vertically aligned and assembled in sheets on a substrate [22,23]. The large surface area of CNW and their good electrical conductivity made them attractive for electrochemical applications. Therefore, coupling ZnO with CNW may offer benefits, such as enhanced faradaic capacitance and electrical conductivity of the composite made of the metal oxide and CNW. Furthermore, the double layer capacitance of the CNW with a large specific surface area can be added to that of ZnO.

In this work, we report the synthesis and electrochemical investigation of carbon nanowall coated with ZnO as electrodes for supercapacitors. The ZnO deposits of different thicknesses were grown on CNW by laser ablation in oxygen reactive atmosphere. The areal capacitance of ZnO was enhanced up to 23 times compared to that of CNW, in mild electrolyte of 1 M KCl with an enhanced cycling stability up to 26,000 cycles. ZnO is already used in solar cells [24] light-emitting diodes [25] and lasing [26]. Therefore, our results pave the road towards the extension of ZnO application for use as promising material for ECs.

2. Experimental

2.1. Synthesis of CNW films

CNW films were grown on (100) silicon substrates by expanding radio frequency (RF) plasma beam. The Ar plasma beam (carrying gas) was injected with acetylene (precursor gas) in the presence of hydrogen (active gas). The ratio of $Ar/H_2/C_2H_2$ was fixed at 1050/25/1 sccm at a pressure of about 100 Pa and RF power of 300 W. During CNW growth, the temperature of the substrate holder was kept at 700 °C. The deposition time was fixed at 10 min in order to obtain CNW films with a thickness of about 500 nm. More experimental details about CNW deposition can be found elsewhere [27].

2.2. Deposition of ZnO on the CNWs

ZnO thin films were deposited on CNW by pulsed laser ablation of Zn target in oxygen reactive atmosphere. The oxygen pressure during irradiation was set at 10^{-2} mbar. During the deposition, the temperature was fixed at 300 °C and the distance target-substrate was kept at 4 cm. More details about the

procedure of ZnO deposition can be found in reference [28]. The resulting composite nanostructured electrodes (CNW-ZnO) are referred to 400 nm, 800 nm and 1200 nm ZnO according to the thickness measured on flat silicon substrates acting as reference samples to calibrate our deposition process.

2.3. Sample characterization

2.3.1. Structural and surface characterization

The samples were characterized using scanning electron microscopy (SEM; JEOL JSM 7500F) at an accelerating voltage of 5 kV. The structural characterization of the samples was performed by X-ray diffraction (XRD) using an X-ray diffractometer D5000 MOXTEK with (Cu Kα) radiation (λ = 0.154 nm) in the ϑ–2ϑ Bragg Brentano configuration. For surface chemical analysis, XPS measurements were carried out on K-Alpha (Thermo Scientific, East Grinstead, England) using a monochromatic (Al Kα) X-ray beam, on a 300 × 300 μm^2 spot area in a spectrometer equipped with a flood gun for charge compensation. The C_{1s} line at 284.4 eV was used as a reference to correct the binding energies for charge energy shift. A Shirley background was subtracted from the spectra and the symmetric Gaussian functions were used during peak-fitting procedure.

2.3.2. Electrochemical characterization

Electrochemical studies of CNW-ZnO electrodes were carried out using a potentiostat/galvanostat PGSTAT128N at room temperature in a typical three-electrode electrochemical cell. The cell is composed of two parts screwed one in each other, one has a copper current collector and the other in Teflon filled with the electrolyte and has a hole at the bottom to enable the contact between the electrode and the electrolyte. The CNW-ZnO samples were used as working electrode, Ag/AgCl as reference electrode and Pt foil as counter electrode. In this cell, only the side coated with CNW-ZnO was in contact with the electrolyte (S = 0.5 cm^2) and the other side was in contact with the current collector by using silver paste to ensure a good contact. The electrodes are characterized by cyclic voltammetry (CV), Galvanostatic ChargeDischarge (GCD) and electrochemical Impedance Spectroscopy (EIS) in KCl (1 M) aqueous solution. Electrochemical Impedance Spectroscopy (EIS) measurements are also carried out at −0.11, 0.03 and 0.07 V vs Ag/AgCl with a signal amplitude V = 10 mV in a frequency range [100 kHz–1 mHz]. Capacitance C of the samples was calculated from cyclic voltammetry and galvanostatic charge-discharge using the following Eqs. (1)–(2) [29,6]:

$$C = \frac{\Delta i}{2v} \quad (1)$$

$$C = \frac{I}{dV/dt} \quad (2)$$

where C is the capacitance, Δi the average of the intensity difference between the upper and the lower part of the cyclic voltammetry curve and v the scan rate. I is the applied current, dV is the potential difference and dt is the discharge time.

3. Results and discussion

The surface morphologies of the CNW and ZnO deposits of different thicknesses (400, 800 and 1200 nm) deposited on CNW are illustrated by SEM images in Fig. 1a–d, respectively. Fig. 1a shows the top view SEM image of CNW layer deposited on a silicon wafer with vertical growth of the carbon sheets and honeycomb structure. Fig. 1b–d reveals that the ZnO deposits are anchored to CNW uniformly on the whole surface. It can be also noticed that the space between walls covered with ZnO decreases when the thickness of ZnO deposit increases (Fig. 1d). In other words, the apparent surface area decreases especially in the case of ZnO deposits with a thickness of 1200 nm. Such results are expected to have an impact on the specific capacitance of CNW-ZnO electrodes. In our case, the nanostructures are deposited on silicon substrates, which means that material quantity available is very low, and therefore, in contrast to powder, the Brunauer-Emmett-Teller (BET) analysis is not possible. The only possible way to estimate the surface area is from SEM images.

XRD patterns of the CNW-ZnO electrodes with different ZnO thicknesses are displayed in Fig. 2. All the peaks of the ZnO deposits can be indexed to the wurtzite single phase ZnO (ASTM No.00-001-1136, a = b = 3.242 Å, c = 5.176 Å, Space group: P63mc, No.186). The distinct peaks can be assigned to (002) and (101) planes of pure ZnO [30]. In the case of ZnO deposited on CNW with thicknesses of 400 and 800 nm, a shift of diffraction peaks position towards lower angles is observed compared to the peaks related to CNW-ZnO with a thickness of 1200 nm. Such a shift towards lower angles, as the thickness of ZnO decreases, can be attributed to stress relaxation in ZnO [30].

The chemical composition and bonding state of the ZnO deposits were investigated by XPS analyses (Fig. 3). The XPS survey spectrum of CNW-ZnO (800 nm thick) indicates the presence of C, O and Zn elements, which confirms the formation of ZnO on the CNW surface (Fig. 3a). The high-resolution XPS spectrum of the Zn_{2p} is presented in (Fig. 3b). It comprises two symmetric peaks at 1021.75 and 1044.65 eV corresponding to $Zn_{2p3/2}$ and $Zn_{2p1/2}$, respectively [1,31–33]. The peak separation between $Zn_{2p3/2}$ and $Zn_{2p1/2}$ is 23.0 eV, in agreement with the previous report for zinc bonded to oxygen [1]. Fig. 3c depicts the high resolution XPS spectrum of the O_{1s} region. It can be deconvoluted into three peaks. The peak at 530.8 eV was attributed to the wurtzite structure of hexagonal Zn^{2+} ion of the metal oxide [31]. The other peaks at 531.7 and 532.5 eV are related to adsorbed oxygen ions in the

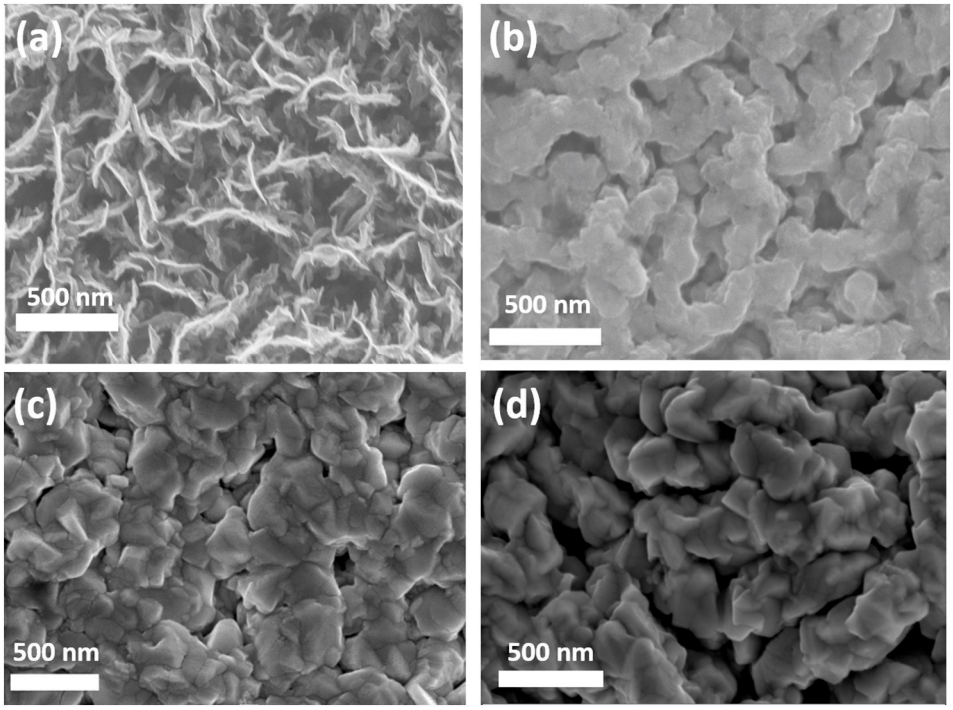

Fig. 1. Top view SEM images of (a) CNWs, (b) CNW-ZnO (with 400 nm thick), (c) CNW-ZnO (with 800 nm thick) and (d) CNW-ZnO (with 1200 nm thick).

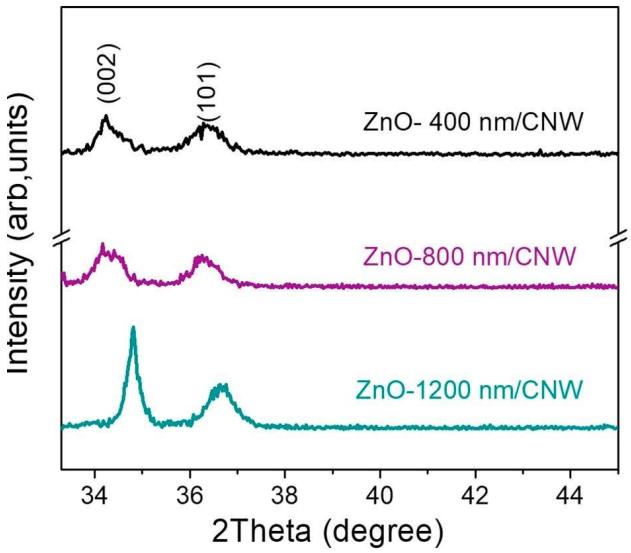

Fig. 2. XRD patterns of CNW-ZnO electrodes with different ZnO thicknesses.

deficient regions [1] and oxygen chemisorbed Oc, respectively [33]. It should be noted that the ZnO deposits contain a large amount of oxygen vacancies compared to oxygen bonded to Zn2+ ions, which may also have an implication on the electrochemical behavior of the electrodes.

The electrochemical performance of prepared CNW-ZnO electrodes was evaluated in a three-electrode configuration by using cyclic voltammetry (CV), galvanostatic charge-discharge (GCD) and electrochemical impedance spectroscopy (EIS) in 1 M KCl aqueous electrolyte. To make a meaningful comparison, the CVs of the CNW and CNW-ZnO electrodes with a thickness of 800 nm were measured at the same scan rate of 50 $mV{\cdot}s^{-1}$. They both exhibit the typical rectangular shape, indicating quasi ideal capacitor (Fig. 4a). The comparison of the CVs of CNW and CNW-ZnO with 800 nm thick ZnO clearly shows that the capacitance current is enhanced in the case of the CNW-ZnO electrode.

The areal capacitance of CNW at 50 $mV{\cdot}s^{-1}$is measured to be 0.19 versus 1.42 $mF{\cdot}cm^{-2}$ for CNW-ZnO electrode. Charge-discharge plots at a current density of 40 $\mu A{\cdot}cm^{-2}$ are displayed in Fig. 4b; they show a symmetric triangular shape, revealing good capacitive behavior of ZnO/CNW electrode, which is consistent with the CV results. ZnO-CNW specific capacitance should be always higher than pristine CNW film without ZnO deposition. This is because ZnO store charges as pseudocapacitive material while CNWs store charges as EDLC materials.

The CV curves of CNW-ZnO electrodes obtained at various scan

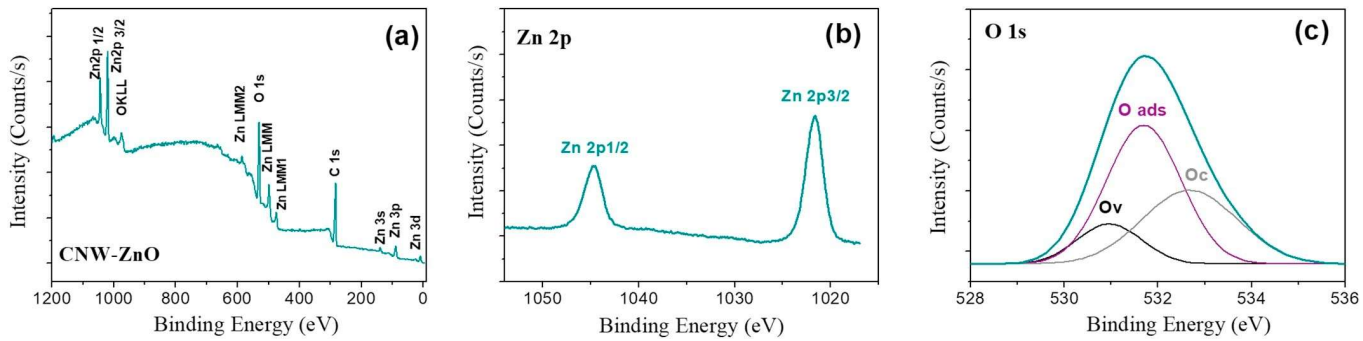

Fig. 3. XPS spectra of ZnO/CNW electrode 800 nm: survey spectrum (a) and high resolution spectra of the Zn_{2p} (b) and O_{1s} (c).

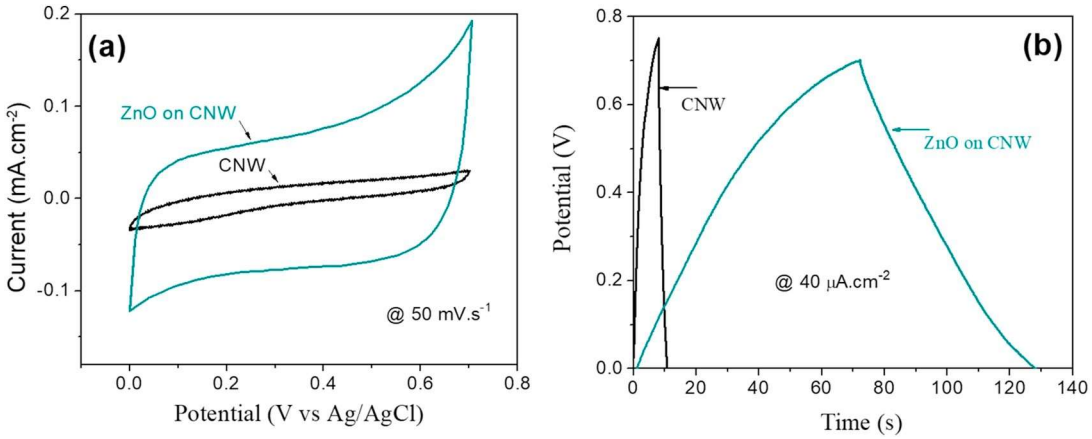

Fig. 4. (a) CV curves of CNW and ZnO-CNW (800 nm thick) electrodes at a scan rate of 50 mV·s^{-1}. (b) Galvanostatic charge-discharge curves at a current density of 40 µA·cm^{-2}.

rates exhibit quasi-rectangular shapes (Fig. 5a–c). The shapes of these curves remain unchanged with increasing the scan rate from 10 to 1000 mVs^{-1}, indicating good capacitive behavior even at high scan rate of 1000 mV·s^{-1}. The CVs curves, however, become more distorted at higher scan rates when the thickness of the ZnO deposit increases. This is more noticeable in the case of CNW-ZnO with a 1200 nm thick layer of ZnO. This indicates that the electrode resistivity increases when the thickness of ZnO increases.

Galvanostatic charge-discharge curves of different CNW-ZnO electrodes with ZnO of different thicknesses at a current density of 40 µA·cm^{-2} are presented in Fig. 6. It can be seen that CNW-ZnO (400–800 nm) electrodes display a small IR drop of 0.01 and 0.009 V, respectively, indicating the superior electrical conductivity of CNWZnO (400–800 nm). Furthermore, CNW and CNW-ZnO 1200 nm electrodes present an IR drop of 0.061 and 0.072 V, respectively, due to the internal resistance of the carbon material and the thick layer of ZnO film (the space between walls narrows when the thickness of ZnO increases) (Fig. 1d).

The areal capacitances of the CNW-ZnO electrodes are calculated from the charge-discharge curves using the Eq. (2); they are found to be 2.35, 3.75 and 0.18 mF·cm^{-2} at a current density of 40 µA·cm^{-2} for CNW-ZnO 400, 800 and 1200 nm, respectively. The CNW electrode exhibits a capacitance of 0.16 mF·cm^{-2}. Thus when compared to CNWZnO (800 nm thick) (3.75 mF·cm^{-2}) at a current density of 40 µA·cm^{-2}, it is obvious that the capacitance is really enhanced by around 23 fold. These results confirm the superior capacitive behavior of the CNW-ZnO nanostructured electrode compared to pristine CNW electrode. Moreover, when compared to other electrodes made of ZnO nanostructures that are reported in literature, the areal capacitance of 4.3 mF·cm^{-2} is higher than or comparable to that of Ref [34] (in the range of 35 µF·cm^{-2}), Ref [35] (in the range of 2.6 mF·cm^{-2}), and much higher

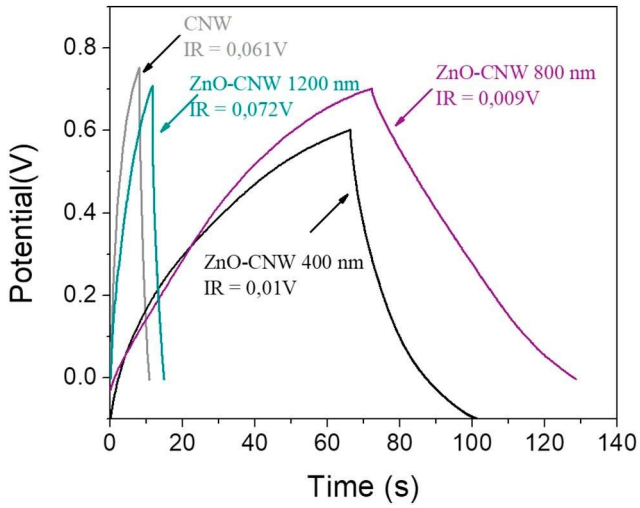

Fig. 6. Galvanostatic charge-discharge curves at a current density of 40 µA·cm^{-2}.

than the corresponding ZnO films, with different thicknesses, deposited on flat silicon substrates as shown in Fig. S1 (in the supporting information).

Fig. 7 depicts the variation of the areal capacitance versus scan rate and current density. It can be seen that the capacitance decreases with increasing the scan rate and current density, suggesting that parts of the surface are inaccessible at high scan and charging-discharging rates. Indeed, as the scan rate increases, the diffusion of electrolyte ion into electrode internal structure and pore become difficult (diffusion

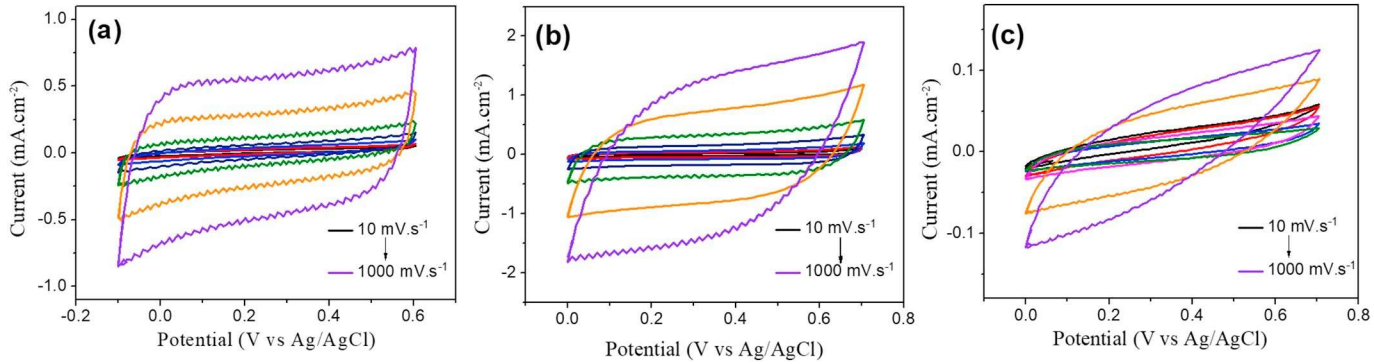

Fig. 5. CV curves at various scan rates. (a) CNW-ZnO400 nm, (b) CNW-ZnO800 nm, (c) CNW-ZnO1200 nm.

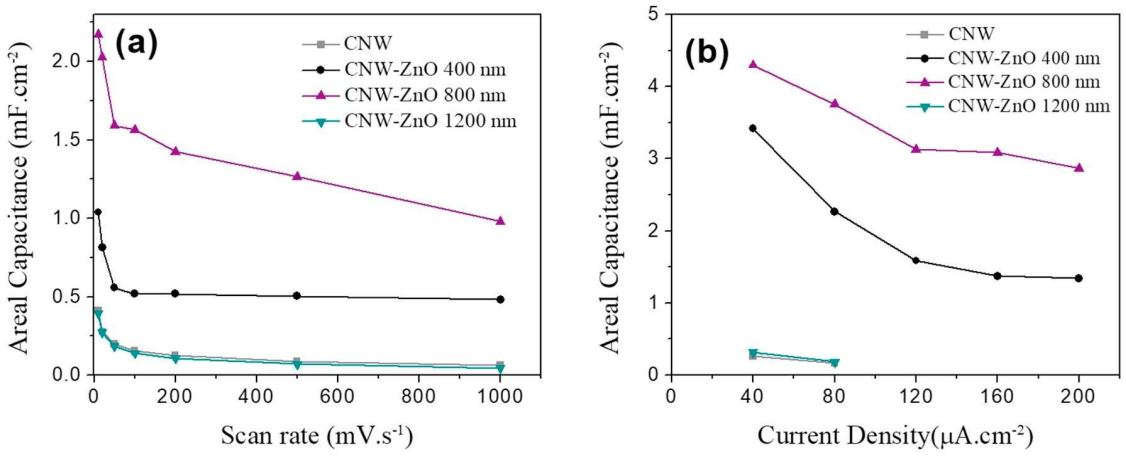

Fig. 7. Variation of areal capacitance: (a) at different scan rates, (b) at different current densities.

limitation) and ineffective interaction between the electrolyte and electrode materials occurs, therefore, the specific capacitance decreases. At low scan rates, there is enough time for ions to penetrate deeply into pores producing high charges and higher specific capacitance. Furthermore, it is clear that the CNW-ZnO (800 nm thick) electrode has the highest capacitance followed by CNW-ZnO (400 nm) and CNW-ZnO (1200 nm); such a behavior can be related to the amounts of ZnO deposits and the surface area of different electrodes, as observed in the SEM images.

EIS measurement were conducted in 1 M KCl aqueous solution at the frequency range of [10 kHz–1 mHz]. Fig. 8 shows the typical Nyquist plots of CNW-ZnO electrodes. A semicircle arc and a straight line are observed. The high frequency arc is attributed to the charge transfer resistance and the double layer capacitance at the interface electrode–electrolyte. The low frequency straight line is due to the diffusion of ions at the electrode–electrolyte interface. The charge transfer resistance (R_{ct}) is calculated from the diameter of high frequency arc to be about 96 Ω, 153 Ω and 505 Ω for CNW-ZnO 400,800 and 1200 nm electrodes respectively. The EIS results are in a good agreement with the CV data presented above for the different electrodes and which indicate that the electrodes become more resistive as the thickness of the ZnO deposit increases.

The cyclic stability is an important parameter in ECs. The cycling stability measurements (Fig. 9) reveal that the areal capacitance of the

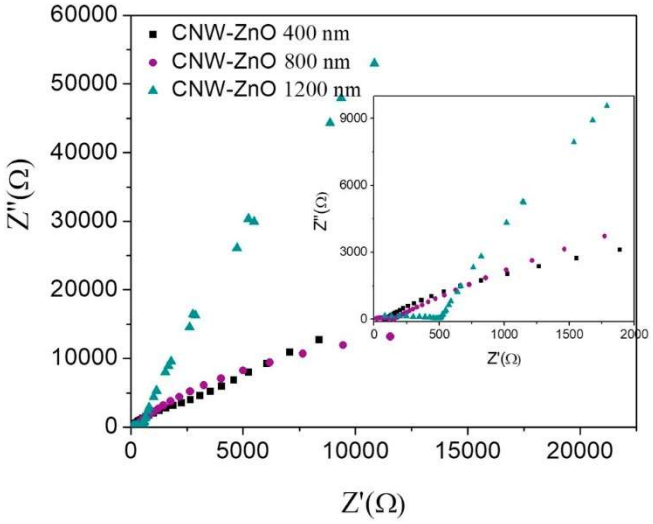

Fig. 8. Nyquist impedance plots for CNW-ZnO (400, 800 and 1200 nm) electrodes.

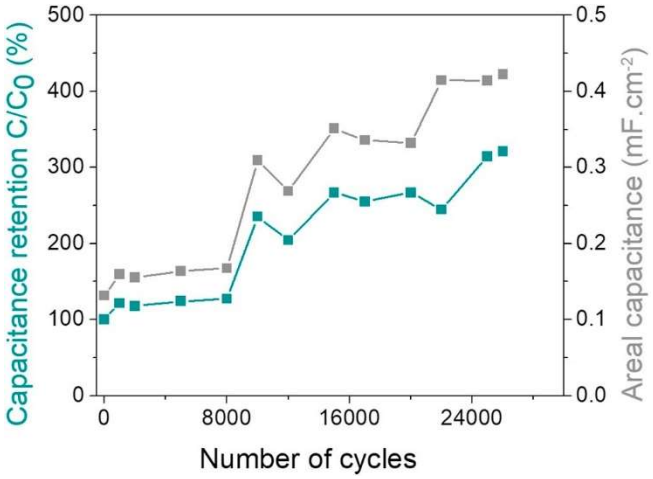

Fig. 9. Evolution of the capacitance for CNW-ZnO800 nm electrode during 26,000 consecutive cycles at scan rate of 100 mV·s^{-1}.

CNW-ZnO electrode (800 nm) increases even after long cycling of 26,000 cycles. To understand this increase in capacity, SEM imaging (Fig. 10) is performed to check the changes on the surface of the electrode after 26,000 cycles. As expected, the surface porosity, of ZnO has been increase after cycling, indicating the dissolution of ZnO; this dissolution is not important since nanowalls remain covered after cycling. The increase in capacity can be explained by the increase of the surface porosity, which leads to the increase of the specific area thus the increase of the specific capacitance [36]. Similar to the present case, in our previous report [37], we have reported the increase of ZnO porosity after cycling due to ZnO dissolution. Indeed, dissolution of the ZnO material happens in both acidic and alkaline baths. The oxygen evolution reaction (Eq. (3)) is supposed to be expected, leading to a localized increase in the proton concentration in the vicinity of the ZnO electrode. This may facilitate the chemical dissolution of the ZnO film via Eq. (5). Thus, there are two competing reactions involving ZnO film dissolution, as described below [38–40].

$$2\,ZnO \rightarrow 2\,Zn^{2+} + O_2 + 4\,e^- \quad (3)$$

$$2\,H_2O \rightarrow 4H^+ + O_2 + 4\,e^- \quad (4)$$

$$2\,ZnO + 4H^+ \rightarrow 2\,ZnOH^+ + 2H^+ \rightarrow 2\,Zn^{2+} + 2\,H_2O \quad (5)$$

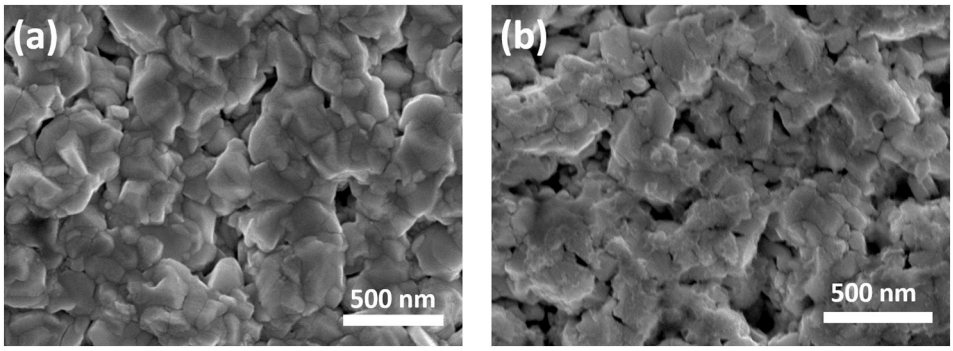

Fig. 10. Top view SEM images of CNW-ZnO (800 nm) (a) before and (b) after 26,000 consecutive cycles.

4. Conclusion

In summary, we reported the synthesis of CNW-ZnO electrodes using expanding radio frequency plasma and laser ablation in oxygen reactive atmosphere. Scanning electron microscopy (SEM) analysis showed that CNW-ZnO samples display a porous honeycombed structure which is advantageous for easy electrolyte access and enhanced charge transfer rate in large area of active electrode materials. Under optimized conditions, the CNW-ZnO (800 nm) electrode exhibits a high areal capacitance of 4.3 $mF{\cdot}cm^{-2}$ at a current density of 0.2 $mA{\cdot}cm^{-2}$ and 1.41 $mF{\cdot}cm^{-2}$ at a scan rate of 10 $mV{\cdot}s^{-1}$ with an enhanced capacitance over 26.000 cycles in mild electrolyte of 1 M KCl. The obtained results suggest that CNW-ZnO can be considered as a promising low cost material for electrochemical capacitors.

Acknowledgements

The authors thank the Wallonia Region for financial support (Project Cleanair; convention 1510618, compl. Feder films). The Synthesis, Irradiation & Analysis of Materials platform of the University of Namur is acknowledged for XPS measurements.

Appendix A. Supplementary data

Supplementary data to this article can be found online at https://doi.org/10.1016/j.apsusc.2019.03.204.

References

[1] X. Xiao, B. Han, G. Chen, L. Wang, Y. Wang, Preparation and electrochemical performances of carbon sphere@ ZnO core-shell nanocomposites for supercapacitor applications, Sci. Rep. 7 (2017) 40167.
[2] Y. Zhang, H. Li, L. Pan, T. Lu, Z. Sun, Capacitive behavior of graphene–ZnO composite film for supercapacitors, J. Electroanal. Chem. 634 (2009) 68–71.
[3] L. Fang, B. Zhang, W. Li, J. Zhang, K. Huang, Q. Zhang, Fabrication of highly dispersed ZnO nanoparticles embedded in graphene nanosheets for high performance supercapacitors, Electrochim. Acta 148 (2014) 164–169.
[4] P. Simon, Y. Gogotsi, Materials for electrochemical capacitors, Nat. Mater. 7 (2008) 845–854.
[5] G. R. Li, Z. L. Wang, F. L. Zheng, Y. N. Ou, Y. X Tong. ZnO@ MoO_3 core/shell nanocables: facile electrochemical synthesis and enhanced supercapacitor performances. Journal of Materials Chemistry, 21 (2011) 4217–4221.
[6] P.M. Kulal, D.P. Dubal, C.D. Lokhande, V.J. Fulari, Chemical synthesis of Fe_2O_3 thin films for supercapacitor application, J. Alloys Compd. 509 (2011) 2567–2571.
[7] S. Hassan, M. Suzuki, A.A. El-Moneim, Capacitive behavior of manganese dioxide/ stainless steel electrodes at different deposition currents, American Journal of Materials Science 2 (2012) 11–14.
[8] J. Yan, E. Khoo, A. Sumboja, P.S. Lee, Facile coating of manganese oxide on tin oxide nanowires with high-performance capacitive behavior, ACS Nano 4 (2010) 4247–4255.
[9] T.M. Dinh, A. Achour, S. Vizireanu, G. Dinescu, L. Nistor, K. Armstrong, D. Guay, D. Pech, Hydrous RuO_2/carbon nanowalls hierarchical structures for all-solid-state ultrahigh-energy-density micro-supercapacitors, Nano Energy 10 (2014) 288–294.
[10] X. Xiao, S. Li, H. Wei, D. Sun, Y. Wu, G. Jin, F. Wang, Y. Zou, Synthesis and characterization of VO_2 (B)/graphene nanocomposite for supercapacitors, J. Mater. Sci. Mater. Electron. 26 (2015) 4226–4233.
[11] X. Xia, D. Chao, C.F. Ng, J. Lin, Z. Fan, H. Zhang, Z.X. Shen, H.J. Fan, VO_2 nanoflake arrays for supercapacitor and Li-ion battery electrodes: performance enhancement by hydrogen molybdenum bronze as an efficient shell material, Materials Horizons 2 (2015) 237–244.
[12] S. Chou, F. Cheng, J. Chen, Electrodeposition synthesis and electrochemical properties of nanostructured γ-MnO_2 films, J. Power Sources 162 (2006) 727–734.
[13] M.S. Wu, Z.S. Guo, J.J. Jow, Highly regulated electrodeposition of needle-like manganese oxide nanofibers on carbon fiber fabric for electrochemical capacitors, J. Phys. Chem. C 114 (2010) 21861–21867.
[14] G.A. Ali, M.M. Yusoff, Y.H. Ng, H.N. Lim, K.F. Chong, Potentiostatic and galvanostatic electrodeposition of manganese oxide for supercapacitor application: a comparison study, Curr. Appl. Phys. 15 (2015) 1143–1147.
[15] S. Hassan, M. Suzuki, S. Mori, A.A. El-Moneim, MnO_2/carbon nanowalls composite electrode for supercapacitor application, J. Power Sources 249 (2014) 21–27. [16] B. Pant, M. Park, P.G. Ouellet, J. Park, Y.S. Kuk, E.J. Lee, S.j. Park. Carbon Nanofibers Wrapped with Zinc Oxide Nano-flakes as Promising Electrode Material for Supercapacitors. Journal of Colloid and Interface Science, 522 (2018) 40–47.
[17] M. Selvakumar, D.K. Bhat, A.M. Aggarwal, S.P. Iyer, G. Sravani, Nano ZnO-activated carbon composite electrodes for supercapacitors, Phys. B Condens. Matter 405 (2010) 2286–2289.
[18] X. He, J.E. Yoo, M.H. Lee, J. Bae, Morphology engineering of ZnO nanostructures for high performance supercapacitors: enhanced electrochemistry of ZnO nanocones compared to ZnO nanowires, Nanotechnology 28 (2017) 245402.
[19] A. Achour, K. Ait Aissa, M. Mbarek, K. El Hadj, N. Ouldhamadouche, N. Barreau, L. Le Brizoual, M.A. Djouadi, Enhancement of near-band edge photoluminescence of ZnO film buffered with TiN, Thin Solid Films 538 (2013) 71–77.
[20] C.H. Kim, B.H. Kim, Zinc oxide/activated carbon nanofiber composites for highperformance supercapacitor electrodes, J. Power Sources 274 (2015) 512–520. [21] A. Achour, J.B. Ducros, R.L. Porto, M. Boujtita, E. Gautron, L. Le Brizoual, T. Brousse, Hierarchical nanocomposite electrodes based on titanium nitride and carbon nanotubes for micro-supercapacitors, Nano Energy 7 (2014) 104–113. [22] A. Achour, B.E. Belkerk, K. Ait Aissa, S. Vizireanu, E. Gautron, M. Carette, M.A. Djouadi, Thermal properties of carbon nanowall layers measured by a pulsed photothermal technique, Appl. Phys. Lett. 102 (2013) 061903.
[23] E.C. Stancu, A.M. Stanciuc, S. Vizireanu, C. Luculescu, L. Moldovan, A. Achour, G. Dinescu, Plasma functionalization of carbon nanowalls and its effect on attachment of fibroblast-like cells, J. Phys. D. Appl. Phys. 47 (2014) 265203.
[24] Z. Zang, Efficiency enhancement of ZnO/Cu2O solar cells with well oriented and micrometer grain sized Cu2O films, Appl. Phys. Lett. 112 (2018) 042106.
[25] Z. Zang, X. Zeng, J. Du, M. Wang, X. Tang, Femtosecond laser direct writing of microholes on roughened ZnO for output power enhancement of InGaN lightemitting diodes, Opt. Lett. 41 (2016) 3463–3466.
[26] C. Li, Z. Zang, C. Han, Z. Hu, X. Tang, J. Du, Y. Leng, K. Sun, Highly compact CsPbBr3 perovskite thin films decorated by ZnO nanoparticles for enhanced random lasing, Nano Energy 40 (2017) 195–202.
[27] A. Achour, S. Vizireanu, G. Dinescu, L. Le Brizoual, M.A. Djouadi, M. Boujtita, Electrochemical anodic oxidation of nitrogen doped carbon nanowall films: X-ray photoelectron and micro-Raman spectroscopy study, Appl. Surf. Sci. 273 (2013) 49–57.
[28] R. Serhane, S. Abdelli-Messaci, S. Lafane, H. Khales, W. Aouimeur, A. Hassein-Bey, T. Boutkedjirt, Pulsed laser deposition of piezoelectric ZnO thin films for bulk acoustic wave devices, Appl. Surf. Sci. 288 (2014) 572–578.
[29] F. Thissandier, P. Gentile, N. Pauc, T. Brousse, G. Bidan, S. Sadki, Tuning silicon nanowires doping level and morphology for highly efficient micro-supercapacitors, Nano Energy 5 (2014) 20–27.
[30] N. Ouldhamadouche, A. Achour, I. Musa, K.A. Aissa, F. Massuyeau, P.Y. Jouan, M. A Djouadi. Structural and photoluminescence characterization of vertically aligned multiwalled carbon nanotubes coated with ZnO by magnetron sputtering. Thin Solid Films, 520 (2012) 4816–4819.

[31] J. Mu, C. Shao, Z. Guo, Z. Zhang, M. Zhang, P. Zhang, Y. Liu, High photocatalytic activity of ZnO-carbon nanofiber heteroarchitectures, ACS Appl. Mater. Interfaces 3 (2011) 590–596.
[32] K.T. Alali, J. Liu, Q. Liu, R. Li, Z. Li, P. Liu, J. Wang, Tube in tube $ZnO/ZnCo_2O_4$ nanostructure synthesized by facile single capillary electrospinning with enhanced ethanol gas-sensing properties, RSC Adv. 7 (2017) 11428–11438.
[33] S.M. Park, T. Ikegami, K. Ebihara, Effects of substrate temperature on the properties of Ga-doped ZnO by pulsed laser deposition, Thin Solid Films 513 (2006) 90–94.
[34] M.A. Borysiewicz, M. Wzorek, M. Ekielski, J. Kaczmarski, T. Wojciechowski, Controlling the nanoscale morphology and structure of the ZnO/MnO_2 system for efficient transparent supercapacitors, MRS Communications 7 (2017) 173–178. [35] M.A. Borysiewicz, M. Ekielski, Z. Ogorzałek, M. Wzorek, J. Kaczmarski, T. Wojciechowski, Highly transparent supercapacitors based on ZnO/MnO_2 nanostructures, Nanoscale 9 (2017) 7577–7587.
[36] P.L. Albinax, J.P. Taberna, P. Cambronne, E. Simon, Flahaut, T. Lebey. Impact of the surface roughness on the electrical capacitance. Microelectronics Journal 37 (2006) 752–758.
[37] A. Achour, M.A. Soussou, K. Ait Aissa, M. Islam, N. Barreau, E. Faulques, L. Le Brizoual, M.A. Djouadi, M. Boujtita, Nanostructuration and band gap emission enhancement of ZnO film via electrochemical anodization, Thin Solid Films 571 (2014) 168–174.
[38] S.E. Pust, J.-P. Becker, J. Worbs, S.O. Klemm, K.J.J. Mayrhofer, J. Hüpkes, Electrochemical etching of zinc oxide for silicon thin film solar cell applications, J. Electrochem. Soc. 158 (2011) 413–419.
[39] Z. Zembura, L. Burzynska, The corrosion of zinc in de-aerated 0.1 M NaCl in the pH range from 1.6 to 13.3, Corros. Sci., 17 (1977) 871–878.
[40] J. Hüpkes, J.I. Owen, S.E. Pust, E. Bunte, Chemical etching of zinc oxide for thinfilm silicon solar cells, Chem. Phys. Chem. 13 (2012) 66–73.